Photodiagnosis and Photodynamic Therapy 26 (2019) 79–84

Contents lists available at ScienceDirect

Photodiagnosis and Photodynamic Therapy

journal homepage: www.elsevier.com/locate/pdpdt

Photodynamic activity and DNA binding studies of $Pd@SiO_2$ core-shell nanoparticles *in vitro*

K.I. Dhanalekshmi[a,*], K. Sangeetha[b], K.S. Meena[b], P. Magesan[a], A. Manikandan[a], K. Jayamoorthy[c]

[a] Dept. of Chemistry, Bharath Institute of Higher Education & Research, Bharath University, Chennai 600 073, Tamil Nadu, India
[b] Dept. of Biotechnology, Bharath Institute of Higher Education & Research, Bharath University, Chennai 600 073, Tamil Nadu, India
[c] Dept. of Chemistry, St. Joseph's College of Engineering, Chennai, Tamil Nadu, India

ARTICLE INFO

Keywords:
$Pd@SiO_2$
Core-shell nanoparticles
HeLa cells
Photodynamic therapy
DNA binding

ABSTRACT

Metal-semiconductor core-shell type $Pd@SiO_2$ nanoparticles (NPs) were successfully synthesized by Stober's method and the product was characterized by UV–vis, XRD, FT-IR, SEM, HR-TEM and EDX techniques. *In vitro* Photodynamic activity and DNA binding studies of $Pd@SiO_2$ core shell nanoparticles were studied. Cell viability of the core-shell nanoparticles against HeLa cell line was screened by MTT assay after exposing at different light doses. The outcome of the present study indicates that the core-shell $Pd@SiO_2$ NPs are highly stable and exhibited strong photodynamic efficiency under LED light illumination in HeLa cells. The results indicated that SiO_2 supported on the surface of Pd NPs not only prevented the aggregation in addition exhibited remarkable photodynamic activity.

1. Introduction

Photodynamic therapy (PDT) has earned interest in the medical community and is recognized as an effective treatment modality. As well, compared to other cancer therapies, PDT may induce immunity, even against less immunogenic tumors, and thus provide better tumor control [1]. PDT is a potentially significant treatment for cancer, along with other recent technological developments [2].

Compared to the bulk materials, noble metal NPs has gained interests because of their size and shape dependent unique optoelectronic properties. Many of these noble metal NPs posses numerous biomedical applications because of their ease of synthesis, characterization and surface functionalization. Noble metal NPs exhibit largely red-shifted properties and that enhances their values in PDT [3–5]. The coating of semiconductor NPs on the surface of the noble metals can make the coated NPs much less toxic and bio-compatible [6,7].

Among the noble metal nanoparticles, Palladium is a widely known nanoparticle. Despite a large number of other NPs are commonly used in diverse biological applications, Pd NPs are not much explored. Particularly, the palladium nanosheet covered hollow mesoporous silica NPs composites was found to particularly deliver the drug and affects cancer cells [8]. Similarly, the palladium complexes containing sulfone and other flexible linkages and chloro groups posses efficient activity against tumor cells [9]. Pd NPs supported on mesoporous silica SBA-15 and MSU-2 is found to show better activity against the cancerous cell lines when compared to the other metal-based complexes supported on mesoporous silicas [10].

Additionally, silica is found to be a better carrier for different anticancer drugs, like gemcitabine and paclitaxel, in the treatment of pancreas cancer in mice. The size- and shape-controllable pores of mesoporous silica NPs (SNPs) can easily store pharmaceutical drugs and prevent their premature release and degradation before reaching their designated target [11]. DNA could be the primary intracellular target for anticancer drugs. Therefore interaction between small molecules and DNA may cause DNA damage in cancer cells, blocking the division of cancer cells, and leading to cell death [12,13]. The use of core-shell NPs in DNA binding studies has been increasing, not just to understand the basics of the interaction models, but due to the gaining importance of core-shell NPs as anti-inflammatory, antifungal, antibacterial or anticancer reagents [14,15].

Hence, in this study, we attempted to synthesize, characterize $Pd@SiO_2$ core-shell NPs and, furthermore, the *in vitro* photodynamic efficiency was evaluated on tumor cells.

2. Materials and methods

2.1. Reagents

Tetraethoxysilane (TEOS), Palladium (II) acetate and Calf Thymus (CT) DNA were obtained from Sigma-Aldrich chemicals. All solvents

* Corresponding author.
E-mail address: dhanamveni88@gmail.com (K.I. Dhanalekshmi).

https://doi.org/10.1016/j.pdpdt.2019.03.008
Received 30 July 2018; Received in revised form 7 March 2019; Accepted 8 March 2019
Available online 09 March 2019

and reagents were purchased commercially from Merck and were used without further purification. Milli–Q type water was used through the entire study.

2.2. Synthesis of core-shell Pd@SiO_2 NPs

Silica nanoparticles were prepared by hydrolysis and condensation of TEOS in ethanol in presence of ammonia as catalyst (Stober's method). Silica particles were prepared by mixing 18 ml of ethanol and 6 ml of TEOS and to that added, dropwise the mixture of 42 ml of ethanol and 9 ml of NH4OH under constant stirring for 5 min. at room temperature. The titration speed was controlled to 20 s per droplet and the stirring was performed continuously for 1 h. The colloidal solution was separated by high speed centrifuge and washed by absolute ethanol for three times to remove residual reactants. On the next day, 0.3 mM Pd (II) acetate was mixed with 90% ethanol solution and to this 7.5 ml of one day old silica colloid was added which was then stirred. The dilute ethanol solution (12 ml) was added dropwise at the titration speed of 14 s per droplet under constant stirring. The resultant solution was again aged for one day. Again, the solution was then centrifuged and washed with water for 3 cycles to remove the residual reactants.

2.3. Characterization

In the present study UV–vis absorption spectra was recorded in a Perkin Elmer Lambda 35 spectrophotometer. X-ray diffraction (XRD) patterns recorded from X'pert PRO PANalytical diffractometer operated with CuK_α radiation (k = 1.5406 Å) source. IR spectroscopic measurements were carried out with a Perkin Elmer FTIR Spectrum RXI spectrometer in the 4000 – 500 cm^{-1} wave-number range using KBr pellets. SEM images were taken from SEM FEI Quanta FEG 200 - Scanning Electron Microscope. Transmission electron microscopy photographs were captured using a JEOL JEM-3010 electron microscope operated at 300 keV with the magnification of 600 and 800 k times. Samples were prepared for transmission electron microscope characterization by dispersing the sample in high purity ethanol, followed by sonication. A drop of this suspension was then evaporated on a copper TEM grid. Samples were then subjected to bright field diffraction contrast imaging experiments to image the particles.

2.4. Cell culture and cell viability in HeLa cells

The human cervical cancer line (HeLa) was obtained from National Centre for Cell Science (NCCS), Pune and grown in Eagles Minimum Essential Medium (EMEM) containing 10% fetal bovine serum. In this study, a total of 2×10^4 HeLa cells/ml was taken in a 2.5 cm diameter wells containing a medium. The cells were maintained at 37 °C in a humidified incubator with 5% CO_2. After 24 h, the cells were treated with the NPs at a concentration of 50, 100, 150 and 200 µg/ml. The plain medium was used as a control. The plates containing HeLa cells were incubated with the NPs in 5% CO_2 atmosphere at 37 °C for 3 h. After incubation, the NPs containing media were removed, and the cells were washed with PBS and then illuminated for different time periods (10, 15, 20, 25 and 30 min) using an LED light source (300 nm). After illumination, PBS was removed, and complete culture medium was added.

The viability of HeLa cells was determined after 3, 8, 12 and 16 h of treatment using the core-shell NPs by MTT assay. 10 µl of the dissolved MTT in PBS (5 mg/ml) was added to each well after treatment with NPs. The resultant formazan crystals were dissolved in dimethyl sulfoxide (200 µl), and the absorbance intensity was measured at 570 nm [16–19]. The control was measured at different concentration of NPs without light irradiation.

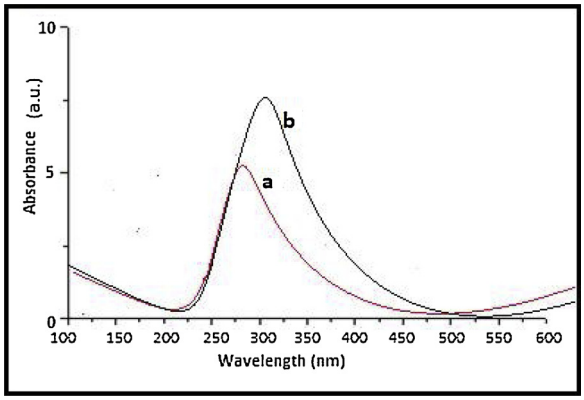

Fig. 1. UV–vis spectrum of Pd@SiO_2 core-shell NPs a) before light irradiation b) after light irradiation (30 min).

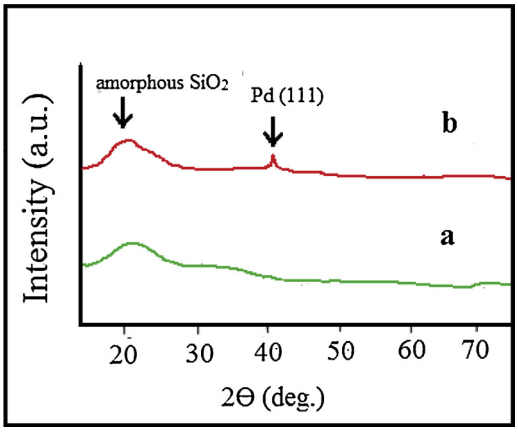

Fig. 2. XRD spectrum of Pd@SiO_2 core-shell NPs a) air dried sample and b) sample annealed at 200 °C.

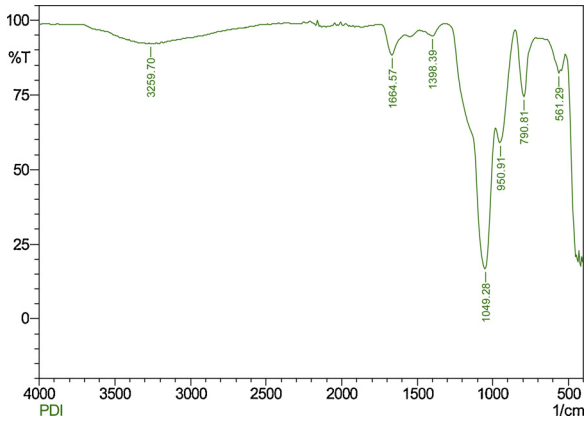

Fig. 3. FT-IR spectrum of Pd@SiO_2 core–shell NPs.

2.5. Cell viability in vero cells

The non toxic concentration and the effect of different light doses were studied in non cancerous *vero cell* line. Cells (1×10^5/ well) were plated in 200 µg/ml of minimum essential medium in 96 well plate to reach the confluency. Different concentrations of the NPs (0 mg/ml to 200 mg/ml) were added to the wells and incubated in 5% CO_2 atmosphere at 37 °C for 3 h. After incubation, the NPs containing media were removed, and the cells were washed with PBS and then illuminated for different time periods (10, 15, 20, 25 and 30 min) using an LED light source (300 nm). After illumination, PBS was removed, and complete

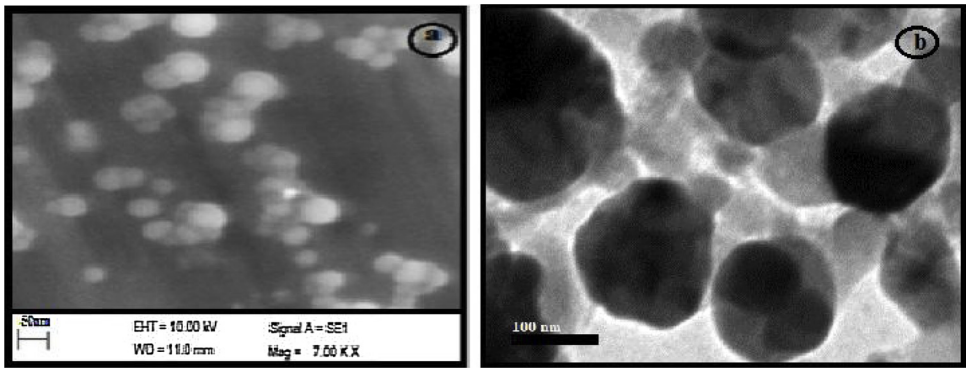

Fig. 4. (a) SEM & (b) TEM images of Pd@SiO_2 core–shell NPs.

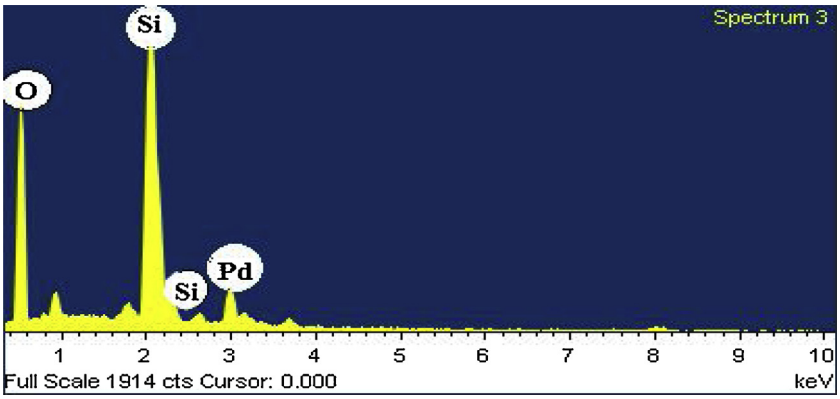

Fig. 5. EDX spectrum of Pd@SiO_2 core–shell NPs.

culture medium was added. MTT assay was performed to the treated cells as described in Section 2.4 after 12 and 24 h of incubation.

2.6. Statistical analysis

The datas were analysed by two way analysis of variance (Annova) followed by Bonferroni post test using Graphpad Prism software V 4.00. The P Value lower than 0.05 were considered statistically significant. All the experiments were performed in triplicates and represented as the mean values with standard errors.

2.7. DNA binding study

By using the UV absorption spectroscopy, the concentration of CT - DNA was determined. The concentration of CT-DNA solution was determined at 260 nm using a mean extinction coefficient value of 6600 $M^{-1}CM^{-1}$. The purity of the solution was determined and it showed that the solution of CT-DNA in the buffer (5 $mmolL^{-1}$Tris-HCl/50 $mmolL^{-1}$NaCl buffer (pH 7.2)) gave a UV absorbance ratio at 260 and 280 nm of approximately 1.89:1 and was free from protein contamination.

At room temperature, the electronic absorption titrations were carried out in DMF (10%) solution of NPs using Tris-HCl/NaCl buffer (5 $mmolL^{-1}$Tris-HCl/50 $mmolL^{-1}$NaCl buffer pH 7.2). Core-shell NPs-DNA solutions were allowed to incubate for 5 min. Then the absorption spectra were determined for different concentrations (0.6×10^{-4}, 0.8×10^{-4} and 1×10^{-3} M DNA) of CT-DNA was determined by keeping the NPs concentration constant.

2.7.1. Calculation of binding constant (K_b)

The binding affinity of core-shell NPs with CT-DNA was calculated from Wolfe–Shimer Eq. (1) [20], through a plot of [DNA]/ε_a–ε_f *vs.* [DNA],

$$[DNA]/\varepsilon_a–\varepsilon_f = [DNA]/\varepsilon_b–\varepsilon_f + 1/K_b| \varepsilon_b–\varepsilon_f 1) \quad l)$$

Where, [DNA] represents the concentration of DNA, Where ε_a is the extinction coefficient observed for the charge transfer absorption at a given DNA concentration, ε_f the extinction coefficient at the NPs free in solution, ε_b the extinction coefficient of the NPs when fully bound to DNA and K_b the equilibrium binding constant.

3. Result and discussion

3.1. UV–vis spectral analysis

UV–vis absorption spectrum of Pd@SiO_2 is shown in Fig. 1. Without light irradiation the NPs showed maximum absorption at 265 nm (Fig. 1(a)). Simultaneous increase of light dose and irradiation time increased the absorption spectrum as shown in Fig. 1(b).

3.2. X-ray diffraction (XRD) analysis

Fig. 2(a, b) illustrate the X-ray diffraction patterns of pre and post-annealed Pd@SiO_2 (at 200 °C in the air for 2 h) NPs respectively. From Fig. 2(a), due to the amorphous SiO_2 support very high broad peak observed at 20°. Different characteristic peak for Pd species was not observed in the XRD pattern recorded at 25 °C, because of the highly dispersed nature of Pd species. After the heat treatment at 200 °C for 2 h (Fig. 2(b)), a slight diffraction peak at 40° is assigned to Pd (111). With increasing temperature during heat treatment, those peaks became stronger and sharper due to the increase in the size of Pd particles. The mean diameter (D) of the particles was calculated using Scherrer's formula. The calculated Pd@SiO_2 core-shell NPs mean size was found to be 42 nm respectively, that matches with the particles size of Pd@SiO_2 calculated by HR-TEM images.

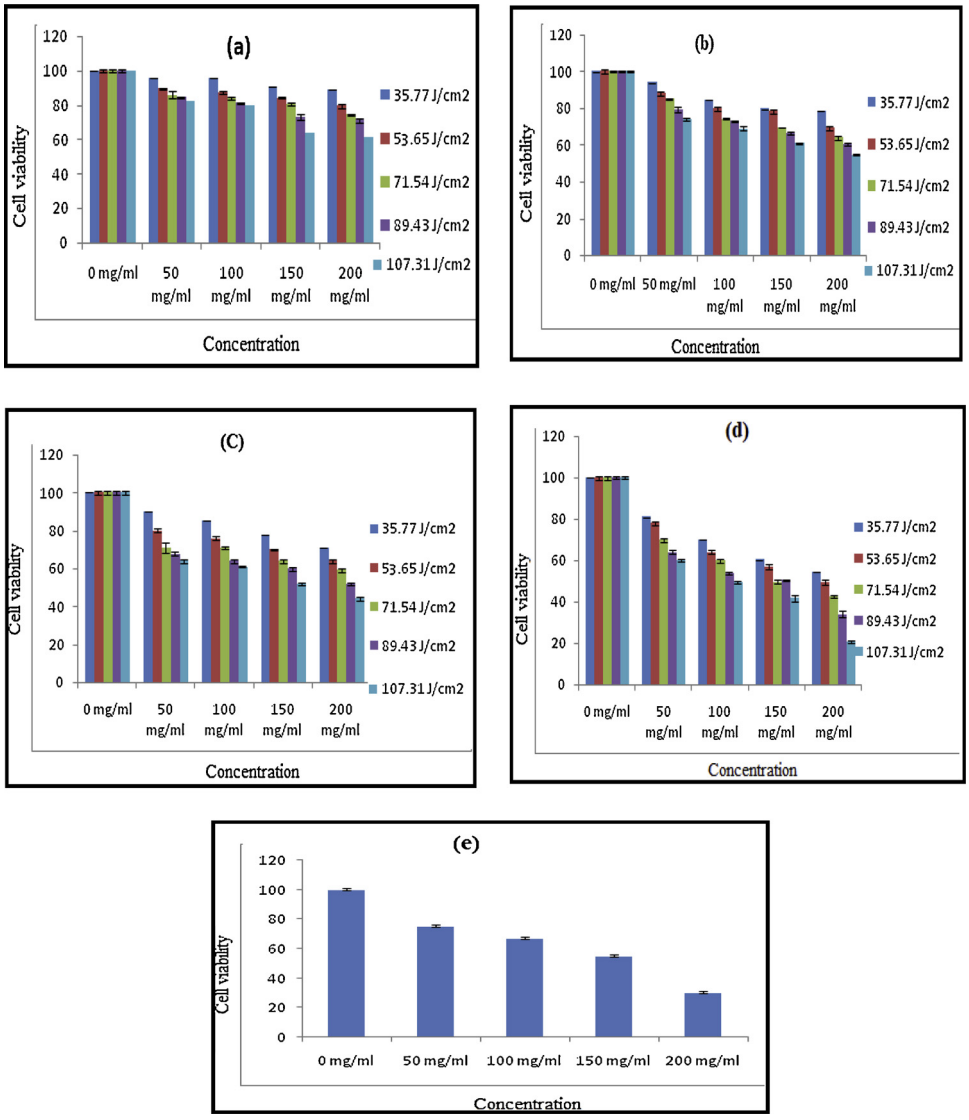

Fig. 6. Effect of light dose and time on cell viability in HeLa cells after a) 3 h, b) 8 h, c) 12 h d) 16 h by Pd@SiO_2 core-shell NPs and e) control without light dose after 16 h of incubation.

3.3. Fourier transform infrared spectroscopy (FT-IR)

Fig. 3 shows the FT-IR spectrum of core-shell Pd@SiO_2 NPs. In FTIR spectra, band observed at 3259 and 1664 cm^{-1} corresponding to O—H stretching and O—H bending vibrations of water molecules, which indicate the hygroscopic character of the powdered samples. The band at 1398 cm^{-1} is due to the CH_2 bending vibration of the solvent molecules. The two peaks at 1049 and 950 cm^{-1} are assigned to the asymmetric stretching vibrations of the Si—O—Si and Si—O (H) bands, and those at 790 and 561 cm^{-1} can be ascribed to the symmetric stretching and bending vibrations of the Si—O—Si bond.

3.4. Scanning electron microscopy (SEM) & Transmission electron microscopy (TEM)

Fig. 4(a) shows the SEM image of core-shell Pd@SiO_2 NPs. The synthesized Pd nanoparticles were nearly spherical and uniform in size, and their diameter increased with the increasing TEOS amount and the average diameter of Pd@SiO_2 NPs was found to be 50 nm. The high ratio of ethanol to water decreases the surface charge as a result of low polarity, which helped complete condensation of TEOS on the NPs surfaces [21].

Fig. 4(b) shows the HR-TEM image of Pd@SiO_2 NPs. A majority is showed by the dark images of Pd core within the size regime. Fig. 4(b) shows the formation of nearly spherical particles of palladium core with a particle diameter of 45–50 nm. There appears some non-uniformity in the shell thickness. The core/shell nanostructures were clearly observed, as a result of the strong contrast between the black cores and gray shells, which confirms the Pd NPs were completely encapsulated with silica shells. The thickness of the SiO_2 shell depends on the coating time and the concentration of TEOS.

3.5. Energy dispersive X-ray analysis (EDX)

EDX spectrum (Fig. 5) indicates that successful deposition of SiO_2 NPs on the Pd surfaces. The EDX result of the coated Pd core with silica shell confirms the presence of Pd, Si and O. Si and O peaks result from the silica shell. No other peaks were detected in the EDX analysis, suggesting the high purity of the core-shell NPs.

3.6. Cell viability

The cytotoxic effect of the nanoparticles at different concentrations, light doses and incubation times on HeLa cells and vero cells were

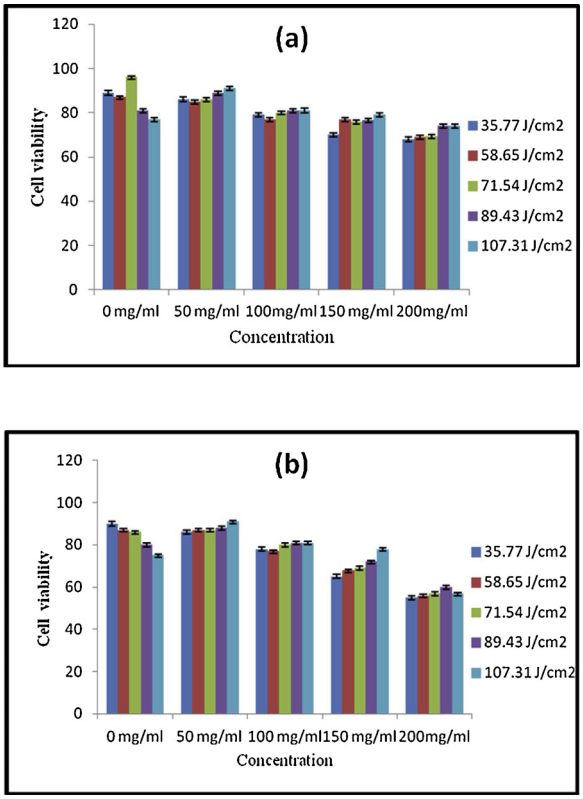

Fig. 7. (a) and (b) Effect of light dose and time on cell viability in *vero cells* after a) 12 h and b) 24 h.

studied by MTT assay. At the tested concentration of 200 mg/ml, the NPs exerted the significant cytotoxic effect of 40% death at the highest light dose of 107.31 J/cm^2. Likewise, the cytotoxic effect increased to two fold by inducing about 80% of cell death after 16 h of incubation. The graph infers that the maximal cytotoxic effect of the NPs was observed at the concentration of 200 mg/ml after 16 h of incubation at the light dose of 107.31 J/cm^2. Besides, it is noteworthy that the induced death is found to be pronounced at the light dose of 71.54 J/cm^2 after 12 h of incubation whereas only a slight change was observed in cytotoxicity activity below 71.54 J/cm^2 at the different tested concentrations of the NPs. Thus increasing the concentration of the NPs to suboptimal levels along with the increased light dose and hours of incubation could influence the cytotoxicity activity in HeLa cells.

There was a significant 50% cell death observed at the concentration of 150 mg/ml in the light dose of 71.54 J/cm^2 after 16 h of incubation (Fig. 6(d)) and this gradually increased to 60% upon an increase in the dose of light to 107.31 J/cm^2. At the 107.31 J/cm^2 light dose after 3 h, 8 h and 12 h the activity has increased from 35, 38 and 48% respectively (Fig. 6a–c). Only about 5 to 10% of the cytotoxic activity was observed until the intensity of 58.65% to 8 h of incubation at the 100 mg/ml concentration. This trend gradually and significantly increased up to 40% after the prolonged incubation period, and the increase in the intensity of light 50% death of HeLa cells occurred at 16 h of incubation at the light dose of 107.31 J/cm^2.

There was no appreciable cytotoxicity activity at the lowest concentration (50 mg/ml). Only a marginal increase in activity observed up to 12 h of incubation, however, the maximum activity of 40% cell death occurred when the incubation period was increased up to 16 h and the light increased to the concentration of 107.31 J/cm^2. Thus both the prolonged incubation period of the NPs and the increase in light dose had exerted a directly proportional cytotoxic effect on the HeLa cells.

Cytotoxic effect of Pd@Sio$_2$ were studied on *vero cells* to determine the maximum non toxic concentration of Nanoparticles and also the

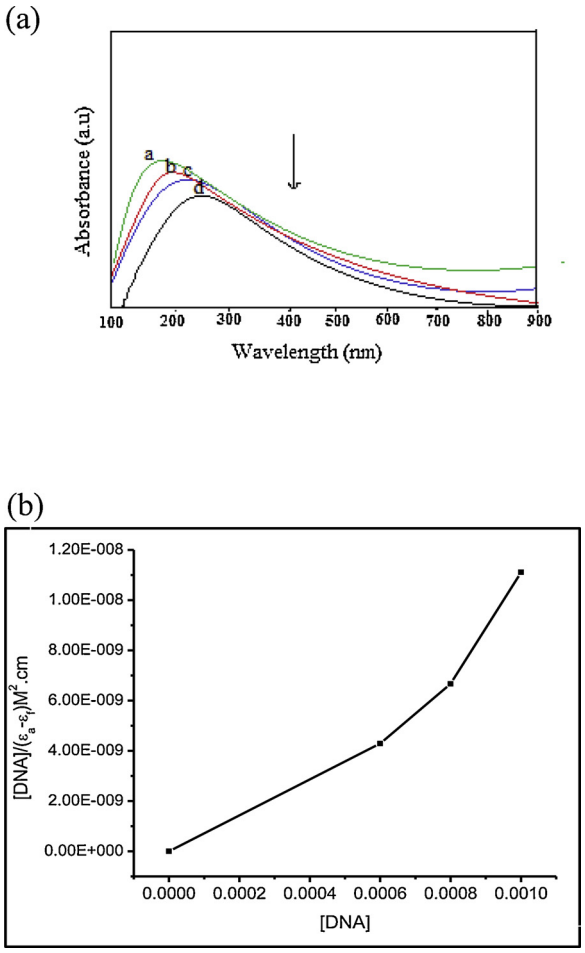

Fig. 8. (a) UV–vis spectrum of Pd@SiO$_2$ NPs (1×10^{-4} M) in 5 mM Tris-HCl buffer with increasing amounts of DNA. a) Free NPs, b) NPs + 0.6×10^{-4} M DNA, c) NPs + 0.8×10^{-4} M DNA andd) NPs + 1×10^{-3} M DNA. (b) Plot for the determination of K_b.

LED illumination effect on normal non cancerous cell lines. At 0 mg/ml concentration of nanoparticles and at the tested various light doses, 90% of cells were viable and this inferred clearly that the light dose both the lower and higher doses studied had not affected the growth of vero cells even after 24 h.

There was a negligible differenc observed at 50 mg/ml and 100 mg/ml concentration after 24 h of incubation. However, the increased nanoparticle concentration at 150 mg/ml and 200 mg/ml decreased the cell viability to 50% after 24 h.

Hence it is obvious that the nanoparticles were highly specific in exerting the cytotoxic effects to the HeLa cells and the higher light dose was non lethal to normal *vero cells* upto 200 mg/ml. It could also be highlighted that below 50 mg/ml, cell survival fraction was found to be increased to 80% and the results are depicted in Fig. 7(a & b).

The nanoparticles at 200 mg/ml after 16 h of incubation at the light dose of 107.31 J/cm^2 exhibited higher activity and were found to significant *** $p < 0.001$. Nanoparticles at 150 and 100 mg/ml had shown the significance of ** $p < 0.01$. However the lowest concentration below 50 mg/ml had shown $p < 0.1$-ns, non significant.

3.7. DNA binding studies

Absorption spectroscopy is among the most useful techniques that are useful to study the binding of any drug to DNA. The interaction of the core-shell NPs with CT - DNA was investigated using the UV absorption spectra of core-shell NPs in the absence and presence of

increasing concentration of DNA and at a constant concentration of the core-shell NPs (Fig. 8a). After the addition of DNA, the changes seen in the UV spectra of the core-shell NPs (either increase or decrease in the intensity or shift in the wavelength) which indicate that the interaction of the core-shell NPs with DNA. It is because of the formation of a new complex with the double-helical DNA [22]. The absorption bands of the core-shell NPs are affected by increasing concentration of DNA. This results in hypochromism with bathochromic shift characterized by the non-covalently intercalative binding of the compound to DNA double helix, due to the strong stacking interaction between the core-shell NPs and base pairs of DNA [23,24]. Titration of DNA with Pd@SiO_2 core-shell nanoparticles showed a hypochromic effect of 38.93% and a bathochromic shift of 42 nm. The number of available intercalation sites becomes more at higher DNA concentration, and the aggregation breaks up favoring intercalative binding of the NPs within the DNA base pairs leading to a further decrease in the absorbance value with a significant bathochromic shift [25,26]. The extent of binding strength of the complexes is quantitatively determined by calculating the intrinsic binding constants K_b of the complexes. This is done by monitoring the change in absorbance at various concentrations of DNA (Fig. 8b). From the plot of [DNA]/($\varepsilon a - \varepsilon f$) *versus* [DNA], K_b values of complexes were determined and found in the range of $4.62 \times 10^4\ M^{-1}$.

4. Conclusions

In conclusion, core shell Pd@SiO_2 NPs were synthesized and characterized. Preliminary studies were performed to identify the NPs as tumor photosensitizer for photodynamic therapy (PDT) in HeLa cells. The nanoparticles were tested in HeLa cells without irradiation as control and the comparative results obtained between the nanoparticles without irradiation and nanoparticles with irradiation had shown marginal difference in the cell viability. The irradiation along with nanoparticles is found to produce an increased marginal death of 10% in HeLa cells. Hence the irradiation could have a considerable effect on the HeLa cells when used in conjugation with nanoparticles. The DNA binding studies revealed the interaction of the nanoparticles and the DNA through intercalation. Further investigations on the DNA interaction studies are warranted to use the Pd@SiO_2 NPs as potential PDTs.

References

[1] T.J. Dougherty, C.J. Gomer, B.W. Henderson, G. Jori, D. Kessel, M. Korbelik, J. Moan, Q. Peng, J. Natl. Cancer Inst. 90 (1998) 889–905.

[2] P. Agostinis, K. Berg, K.A. Cengel, T.H. Foster, A.W. Girotti, S.O. Gollnick, S.M. Hahn, M.R. Hamblin, A. Juzeniene, D. Kessel, M. Korbelik, J. Moan, P. Mroz, D. Nowis, J. Piette, B.C. Wilson, J. Golab, Photodynamic therapy of cancer: an update, CA Cancer J. Clin. 61 (2011) 250–281.

[3] L.R. Hirsch, R.J. Stafford, J.A. Bankson, S.R. Sershen, B. Rivera, R.E. Price, Nanoshell-mediated near-infrared thermal therapy of tumors under magnetic resonance guidance, Proc. Natl. Acad. Sci. U. S. A. 100 (2003) 13549–13554.

[4] X. Huang, I.H. El-Sayed, W. Qian, M.A. El-Sayed, Cancer cell imaging and photothermal therapy in the near-infrared region by using gold nanorods, J. Am. Chem. Soc. 128 (2006) 2115–2120.

[5] J. Chen, D. Wang, J. Xi, L. Au, A. Siekkinen, A. Warsen, et al., Immuno gold nanocages with tailored optical properties for the targeted photothermal destruction of cancer cells, Nano Lett. 7 (2007) 1318–1322.

[6] H. Zheng, Y. Tan, Z. Chen, G. Li, X. Shu, H. Guo, Evolution mechanism of interface cohesion for the coating inducing by laser cladding YSZ@Ni core-shell nanoparticles: Experimental and theoretical research, J. Alloys Compd. 708 (2017) 844–852.

[7] C. Neela Mohan, V. Renuga, A. Manikandan, Influence of silver precursor concentration on structural, optical and morphological properties of $Cu_{1-x}Ag_xInS_2$ semiconductor nanocrystals, J. Alloys Compd. 729 (2017) 407–417.

[8] W. Fang, S. Tang, P. Liu, X. Fang, J. Gong, N. Zheng, Pd nanosheet-covered hollow mesoporous silica nanoparticles as a platform for the chemo-photothermal treatment of cancer cells, Small 8 (2012) 3816–3822.

[9] A.F. Elhusseiny, H.H.A.M. Hassan, Antimicrobial and antitumor activity of platinum and palladium complexes of novel spherical aramides nanoparticles containing flexibilizing linkages: structure-property relationship, Spectrochim. Acta A 103 (2013) 232–245.

[10] A. Balbin, F. Gaballo, J.C. Torres, S. Prashar, M. Fajardo, G.N. Kaluderovic, S.G. Ruiz, Dual application of Pd nanoparticles supported on mesoporous silica SBA-15 and MSU-2: supported catalysts for C–C coupling reactions and cytotoxic agents against human cancer cell lines, RSC Adv. 4 (2014) 54775–54787.

[11] H. Meng, M. Wang, H. Liu, X. Liu, A. Situ, B. Wu, Z. Ji, C.H. Chang, A.E. Nel, Use of a lipid-coated mesoporous silica nanoparticle platform for synergistic gemcitabine and paclitaxel delivery to human pancreatic cancer in mice, ACS Nano 9 (2015) 3540–3557.

[12] G. Zuber, J.C. Quada, S.M. Hecht Jr, Sequence selective cleavage of a DNA octanucleotide by chlorinated bithiazoles and bleomycins, J. Am. Soc. Chem 120 (1998) 9368.

[13] S.M. Hecht, Bleomycin: new perspectives on the mechanism of action, J. Nat. Prod. 63 (158) (2000).

[14] J.R.J. Sorenson, G. Berthon (Eds.), Handbook on Metal–Ligand Interactions in Biological Fluids: Bioinorganic Medicine, 2 Marcel Dekker, New York, 1995, p. 1128.

[15] A. Manikandan, E. Manikandan, B. Meenatchi, S. Vadivel, S.K. Jaganathan, R. Ladchumananandasivam, M. Henini, M. Maaza, J.S. Aanand, Rare earth element (REE) lanthanam doped zinc oxide (La: ZnO) nanomaterials: synthesis structural optical and antibacterial studies, J. Alloys Compd. 723 (2017) 1155–1161.

[16] T. Mossman, A rapid colorimetric assay for cellular growth and survival: application to proliferation and cytotoxicity assays, J. Immun. Method 65 (1983) 55–63.

[17] I. Roy, T.Y. Ohulchanskyy, H.E. Pudavar, Ceramic-based nanoparticles entrapping water-insoluble photosensitizing anticancer drugs: a novel drug—carrier system for photodynamic therapy, J. Am. Chem. Soc. 125 (2003) 7860–7865.

[18] R.W.K. Wu, C.M.N. Yow, C.K. Wong, Y.H. Lam, Photodynamic therapy (PDT)-initiation of apoptosis via activation of stress-activatedp38 MAPK and JNK signal pathway in H460 cell lines, Photodiagnosis Photodyn. Ther. 8 (2011) 254–263.

[19] E.S.M. Chu, C.M.N. Yow, Modulation of telomerase and signal trans-duction proteins by Hexyl-ALA-photodynamic therapy (PDT) inhuman doxorubicin-resistant cancer cell models, Photodiagnosis Photodyn. Ther. 9 (2012) 243–255.

[20] A. Wolfe, G.H. Shimmer, T. Meehan, Polycyclic aromatic hydrocarbons physically intercalate into duplex regions of denatured DNA, Biochemistry 26 (1987) 6392–6396.

[21] L.M. Liz-Marzan, M. Giersig, P. Mulvaney, Synthesis of nanosized gold-silica core-shell particles, Langmuir 12 (1996) 4329–4335.

[22] N.M. El-Metwaly, Spectral and biological investigation of 5-hydroxyl-3-oxopyrazoline 1-carbothiohydrazide and its transition metal complexes, Trans. Met. Chem. 32 (2007) 8.

[23] J.K. Barton, A.T. Danishefsky, J.M. Goldberg, Tris(phenanthroline)ruthenium(II): stereoselectivity in binding to DNA, J. Am. Chem. Soc. 106 (1984) 2172–2176.

[24] H.K. Lu, J.J. Liang, Z.Z. Zeng, P.X. Xi, X.H. Liu, F.J. Chen, Z.H. Xu, Trans. Metal. Chem. 32 (2007) 564–569.

[25] W. Lu, D.A. Vicic, J.K. Barton, Reductive and oxidative DNA damage by photoactive platinum (II) intercalators, Inorg. Chem. 44 (2005) 7970–7980.

[26] M.L. Clark, R.L. Green, O.E. Johnson, P.E. Fanwick, D.R. McMillin, DNA-Binding and physical studies of Pt (4′-NR2-trpy) CN^+ systems (trpy = 2, 2′: 6′, 2″-Terpyridine), Inorg. Chem. 47 (2008) 9410–9494.